structural function. Such materials will increase the reliability and service life of thermosetting polymers used in a wide variety of applications ranging from microelectronics to aerospace. These concepts may also be applicable to a broad class of brittle materials including ceramics and glasses. We expect that the field of self-healing, although still in its infancy, will evolve beyond the method presented here until true biomimetic healing is achieved by incorporating a circulatory system that continuously transports the necessary chemicals and building blocks of healing to the site of damage. □

Methods

Preparation of microcapsules by *in situ* polymerization

In a 600 ml beaker we dissolved urea (0.11 mol, 7.0 g) followed by resorcinol (0.5 g) and ammonium chloride (0.5 g) in water (150 ml). A 5 wt.% solution of ethylene maleic anhydride copolymer (100 ml) was added to the reaction mixture and the pH of the reaction mixture was adjusted to 3.5 using 10% NaOH solution. The reaction mixture was agitated at 454 r.p.m. and to the stirred solution we added 60 ml of dicyclopentadiene to achieve an average droplet size of 200 μm. To the agitated emulsion was added 37% formaldehyde (0.23 ml, 18.91 g) solution and then the temperature of the reaction mixture was raised to 50 °C and maintained for 2 h. After 2 h, 200 ml of water was added to the reaction mixture. After 4 h, the reaction mixture was cooled to room temperature and the microcapsules were separated. The microcapsule slurry was diluted with an additional 200 ml of water and washed with water (3 × 500 ml). The capsules were isolated by vacuum filtration, and air dried. The yield was 80%. Their average size was 220 μm.]

Self-healing epoxy specimen manufacture

The epoxy matrix composite was prepared by mixing 100 parts EPON 828 (Shell Chemicals Inc.) epoxide with 12 parts DETA (diethylenetriamine) curing agent (Shell Chemicals Inc.). Self-healing epoxy specimens were prepared by mixing 2.5% (by weight) Grubbs' catalyst and 10% (by weight) microcapsules with the resin mixture described above. The resin was then poured into silicone rubber moulds and cured for 24 h at room temperature, followed by postcuring at 40 °C for 24 h.

TDCB specimens

The TDCB sample was introduced by Mostovoy and co-workers[23] and is designed so that the compliance of the specimen changes linearly with crack length during the test. This tapered geometry enables controlled crack growth across the centre of a brittle sample such as epoxy. The fracture toughness for TDCB specimens depends only on the applied load and is independent of the crack length so that $K_{IC} = \alpha P_c$ where α is a function of geometry and material properties and P_c is the critical load at fracture. K_{IC} is the experimentally determined mode-I critical stress intensity factor. A taper angle of 40° was used and α was measured to be 7,700 $m^{-3/2}$.

Quantifying healing efficiency

Previous studies of crack healing in thermoplastic polymers quantified healing effects by comparing the fracture toughness of the virgin material to the fracture toughness measured after crack closure and healing.[13–16]. An efficiency of healing was defined as the ratio of the fracture toughness of healed and virgin materials such that $\eta = K_{IC}^{healed}/K_{IC}^{virgin}$ where η is the healing efficiency.

Received 15 August; accepted 12 December 2000.

1. Talrega, R. Damage development in composites: mechanisms and modelling. *J. Strain Anal. Eng. Des.* **24,** 215–222 (1989).
2. Talrega, R. (ed.) *Damage Mechanics of Composite Materials* 139–241 (Elsevier, New York, 1994).
3. Gamstedt, E. K. & Talrega, R. Fatigue damage mechanisms in unidirectional carbon-fibre-reinforced plastics. *J. Mater. Sci.* **34,** 2535–2546 (1999).
4. Pecht, M. G., Nguyen, L. T. & Hackim, E. B. *Plastic-Encapsulated Microelectronics* 235–301 (John Wiley & Sons, New York, 1995).
5. Lee, L. H. *Adhesive Bonding* 239–291 (Plenum, New York, 1991).
6. Wool, R. P. *Polymer Interfaces: Structure and Strength* Ch. 12 445–479 (Hanser Gardner, Cincinnati, 1995).
7. Dry, C. & Sottos, N. in *Smart Structures and Materials 1993: Smart Materials* (ed. Varadan, V. K.) Vol. 1916, 438 (SPIE Proceedings, SPIE, Bellingham, WA, 1993).
8. Dry, C. Procedures developed for self-repair of polymeric matrix composite materials. *Comp. Struct.* **35,** 263–269 (1996).
9. Wiederhorn, S. M. & Townsend, P. R. Crack healing in glass. *J. Am. Ceram. Soc.* **53,** 486–489 (1970).
10. Stavrinidis, B. & Holloway, D. G. Crack healing in glass. *Phys. Chem. Glasses* **24,** 19–25 (1983).
11. Inagaki, M., Urashima, K., Toyomasu, S., Goto, Y. & Sakai, M. Work of fracture and crack healing in glass. *J. Am. Ceram. Soc.* **68,** 704–706 (1985).
12. Jud, K. & Kausch, H. H. Load transfer through chain molecules after interpenetration at interfaces. *Polym. Bull.* **1,** 697–707 (1979).
13. Jud, K., Kausch, H. H. & Williams, J. G. Fracture mechanics studies of crack healing and welding of polymers. *J. Mater. Sci.* **16,** 204–210 (1981).
14. Kausch, H. H. & Jud, K. Molecular aspects of crack formation and healthy in glassy polymers. *Plastic Rubber Proc. Appl.* **2,** 265–268 (1982).
15. Wool, R. P. & O'Conner, K. M. A theory of crack healing in polymers. *J. Appl. Phys.* **52,** 5953–5963 (1982).
16. Wang, E. P., Lee, S. & Harmon, J. Ethanol-induced crack healing in poly(methyl methacrylate). *J. Polym. Sci. B* **32,** 1217–1227 (1994).
17. Lin, C. B., Lee, S. & Liu, K. S. Methanol-induced crack healing in poly(methyl methacrylate). *Polym. Eng. Sci.* **30,** 1399–1406 (1990).
18. Raghavan, J. & Wool, R. P. Interfaces in repair, recycling, joining and manufacturing of polymers and polymer composites. *J. Appl. Polym. Sci.* **71,** 775–785 (1999).
19. Mura, T. *Micromechanics of Defects in Solids* 2nd edn (Kluwer Academic, New York, 1987).
20. Grubbs, R. H. & Tumas, W. Polymer synthesis and organotransition metal chemistry. *Science* **243,** 907–915 (1989).
21. Schwab, P., Grubbs, R. H. & Ziller, J. W. Synthesis and applications of $RuCl_2(=CHR')(PR_3)_2$: the influence of the alkylidene moiety on metathesis activity. *J. Am. Chem. Soc.* **118,** 100–110 (1996).
22. Sanford, M. S., Henling, L. M. & Grubbs, R. H. Synthesis and reactivity of neutral and cationic ruthenium(II) tri(pyrazolyl)borate alkylidenes. *Organometallics* **17,** 5384–5389 (1998).
23. Mostovoy, S., Croseley, P. B. & Ripling, E. J. Use of crack-line-loaded specimens for measuring plane-strain fracture toughness. *J. Mater.* **2,** 661–681 (1967).

Acknowledgements

This work has been sponsored by the University of Illinois Critical Research Initiative Program and the AFOSR Aerospace and Materials Science Directorate. Electron microscopy was carried out in the Center for Microanalysis of Materials, University of Illinois, which is supported by the US Department of Energy.

Correspondence and requests for materials should be addressed to S.W. (e-mail: swhite@uiuc.edu).

A chiroselective peptide replicator

Alan Saghatelian, Yohei Yokobayashi, Kathy Soltani & M. Reza Ghadiri

Departments of Chemistry and Molecular Biology and the Skaggs Institute for Chemical Biology, The Scripps Research Institute, La Jolla, California 92037, USA

The origin of homochirality in living systems is often attributed to the generation of enantiomeric differences in a pool of chiral prebiotic molecules[1,2], but none of the possible physiochemical processes considered[1–7] can produce the significant imbalance required if homochiral biopolymers are to result from simple coupling of suitable precursor molecules. This implies a central role either for additional processes that can selectively amplify an initially minute enantiomeric difference in the starting material[1,8–12], or for a nonenzymatic process by which biopolymers undergo chiroselective molecular replication[13–16]. Given that molecular self-replication and the capacity for selection are necessary conditions for the emergence of life, chiroselective replication of biopolymers seems a particularly attractive process for explaining homochirality in nature[13–16]. Here we report that a 32-residue peptide replicator, designed according to our earlier principles[17–20], is capable of efficiently amplifying homochiral products from a racemic mixture of peptide fragments through a chiroselective autocatalytic cycle. The chiroselective amplification process discriminates between structures possessing even single stereochemical mutations within otherwise homochiral sequences. Moreover, the system exhibits a dynamic stereochemical 'editing' function; in contrast to the previously observed error correction[20], it makes use of heterochiral sequences that arise through uncatalysed background reactions to catalyse the production of the homochiral product. These results support the idea that self-replicating polypeptides could have played a key role in the origin of homochirality on Earth.

Chiroselective amplification refers to an autocatalytic process in which a homochiral template instructs the synthesis of a homochiral polymer of the same handedness[13]. Past efforts aimed at establishing the feasibility of nonenzymatic chiroselective amplification, using nucleic acids and their analogues, have been hampered by lack of template turnover[13] and/or enantiomeric cross-inhibition processes in template-directed oligomerization of activated monomeric building blocks[14–16].

The peptide used in the present study was identified using design and mechanistic principles that are similar to previously

described systems[17–20]. An enantiomeric pair of electrophilic E and nucleophilic N peptide fragments was employed in order to probe the relationship between self-replication and homochirality (Fig. 1). Each pair of electrophile or nucleophile contains one member that is composed of entirely L amino acids, N^L and E^L, and the other contains only unnatural D amino acids, N^D and E^D. Reactions between these four substrates can give rise to four possible products: homochiral templates, T^{LL} and T^{DD}, or heterochiral products, T^{LD} and T^{DL} (Fig. 2).

From a 'racemic' starting mixture made up of equal amounts of electrophilic (E^D and E^L) and nucleophilic (N^L and N^D) fragments, homochiral products (T^{LL} and T^{DD}) are preferentially produced (Fig. 3a). Product formation and diminution of starting materials were monitored by reverse-phase high-performance liquid chromatography (RP-HPLC) and validated by mass spectrometry and HPLC retention time comparisons with authentic materials. The observed generation of increasing diastereomeric excess during the course of the reaction is due to the autocatalytic activity of the homochiral templates, which initially appear in the reaction mixture along with the heterochiral products through uncatalysed background coupling reactions (Fig. 3b). To study the mechanism of chiroselective amplification, we systematically analysed the various steps involved in product formation.

First we examined the degree of inherent stereoselectivity in the fragment condensation reactions[21] which can be studied only in the absence of template control (interhelical noncovalent interactions) and other biasing structural factors. Thus a 'racemic' mixture of the four fragments were allowed to react in buffered solutions containing 3 M GndHCl to ensure denaturation of catalytically competent intermolecular complexes.

Both homochiral and heterochiral products were produced at the same rate, indicating that the ligation chemistry was not inherently diastereoselective (Fig. 3a). Therefore, the selective amplification of homochiral products under native (non-denaturing) reaction conditions is the direct result of chiroselective autocatalysis (Fig. 2).

To further investigate the chiroselectivity and examine the possibility of cross-isomer inhibition, two sets of reactions were performed where the only possible product was either homochiral or heterochiral (reactions 1–4). In one series, we examined the possible catalytic, autocatalytic, and/or inhibitory effects of the four products on the rate of T^{LL} production (reaction 2).

$$E^L + N^L \xrightarrow{T^{LL}} T^{LL} \quad (1)$$

$$E^L + N^L \xrightarrow{T^{LL},T^{DD},T^{LD},T^{DL}} T^{LL} \quad (2)$$

$$E^D + N^L \xrightarrow{T^{LL},T^{DD},T^{LD},T^{DL}} T^{DL} \quad (3)$$

$$E^D + N^L \xrightarrow{\text{No templates}} T^{DL} \quad (4)$$

$$E^L + E^D + N^L \xrightarrow{T^{LL}} T^{DL} + T^{LL} \quad (5)$$

T^{LL} autocatalytically accelerates its own production in reaction mixtures containing equimolar amounts of N^L and E^L (reaction 1; Fig. 3c), and adding T^{DD}, T^{DL} or T^{LD} individually did not have any observable influence on the rate of T^{LL} production. Indeed, reactions between N^L and E^L in the presence of equimolar amounts of all four templates, T^{LL}, T^{DD}, T^{DL} and T^{DL} (reaction 2), displayed a

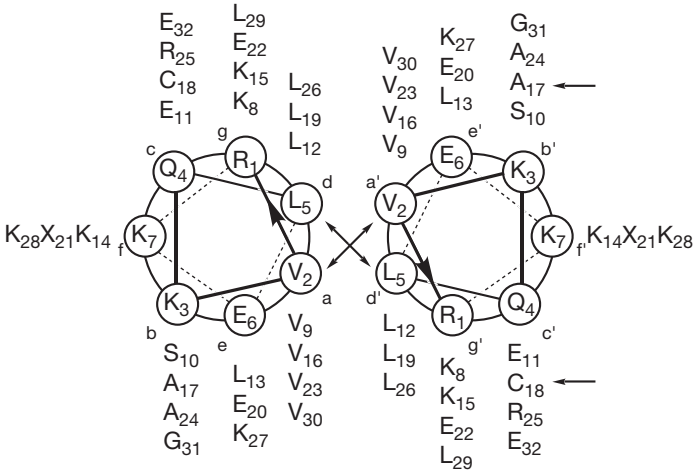

T^{LL}	Ar-RVKQLEKKVSELLKKVACLEXEVARLKKLVGE-$CONH_2$
T^{DD}	Ar-**RVKQLEKKVSELLKKVACLEXEVARLKKLVGE**-$CONH_2$
T^{LD}	Ar-RVKQLEKKVSELLKKVA**CLEXEVARLKKLVGE**-$CONH_2$
T^{DL}	Ar-**RVKQLEKKVSELLKKVA**CLEXEVARLKKLVGE-$CONH_2$
$T^{LL}_{d\text{Leu26}}$	Ar-RVKQLEKKVSELLKKVACLEXEVAR**L**KKLVGE-$CONH_2$
$T^{LL}_{d\text{Arg25}}$	Ar-RVKQLEKKVSELLKKVACLEXEVA**R**LKKLVGE-$CONH_2$
$T^{LL}_{d\text{Cys18}}$	Ar-RVKQLEKKVSELLKKVA**C**LEXEVARLKKLVGE-$CONH_2$
T^{LL}-SH	Ar-CGGRVKQLEKKVSELLKKVACLEXEVARLKKLVGE-$CONH_2$
T^{DD}-SH	Ar-**CGGRVKQLEKKVSELLKKVACLEXEVARLKKLVGE**-$CONH_2$
E^L	Ar-RVKQLEKKVSELLKKVA-COSBn
E^D	Ar-**RVKQLEKKVSELLKKVA**-COSBn
N^L	CLEXEVARLKKLVGE-$CONH_2$
N^D	**CLEXEVARLKKLVGE**-$CONH_2$
$N^L_{d\text{Leu26}}$	CLEXEVAR**L**KKLVGE-$CONH_2$
$N^L_{d\text{Arg25}}$	CLEXEVA**R**LKKLVGE-$CONH_2$
$N^L_{d\text{Cys18}}$	**C**LEXEVARLKKLVGE-$CONH_2$

Figure 1 Helical wheel diagram and peptide sequences employed in this study. The chiroselective peptide replicator is shown in a homodimeric coiled-coil state with arrows representing the ligation site at the solvent-exposed helical surface. Amino acid residues at the a, d, e and g positions compose the interhelical recognition interace. Amino acid residues with D configuration are shown in bold. Bn, benzyl; Ar, 4-acetamidobenzoyl; and X, lysine-ϵ-NHCO-Ar.

similar rate of product formation to that of the reaction where T^{LL} was the only template present (Fig. 3c). These experiments suggest that T^{LL} is the only active template involved in the ligation of E^L and N^L, and that all the other templates (enantiomer and diastereomers) act only as spectators during the formation of T^{LL} (Fig. 3c).

When the fragments N^L and E^D are reacted to study the production of the heterochiral template T^{LD}, the reaction rates are largely the same as in the presence (reaction 3) and absence (reaction 4) of any or all of the four templates (Fig. 3c). These experiments indicate that the heterochiral products are produced in a template-independent fashion largely through uncatalysed bimolecular background reactions. Thus the homochiral templates are highly chiroselective autocatalysts that neither inhibit nor promote the ligation of the other products studied.

The possibility of substrate-mediated enantiomeric cross-inhibition[14–16] was examined by comparing the rates of T^{LL} formation in reactions 1 and 5 under similar reaction conditions. Analyses of reaction mixtures containing equimolar amounts of E^L, N^L and 30 mole% T^{LL} either in the absence (reaction 1) or presence of equimolar amounts of E^D (reaction 5) gave similar rates of T^{LL} production, thus demonstrating the absence of enantiomeric cross-inhibition in the self-replication process.

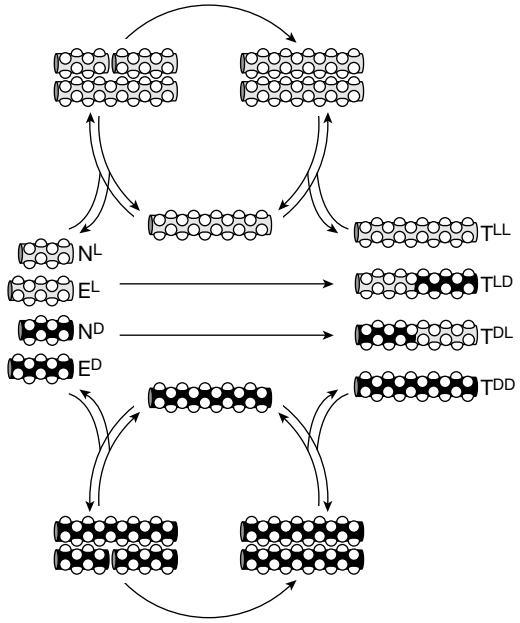

Figure 2 A schematic representation of the chiroselective replication cycles. Homochiral peptides T^{LL} and T^{DD} are produced autocatalytically[17,18] while the heterochiral peptides T^{DL} and T^{DL} result from uncatalysed background fragment condensation reactions[27]. Template-directed ligation reactions proceed through the intermediary of stereospecific noncovalent complexes (ternary and/or quaternary) and pass the stereochemical information from the homochiral products to the substrates, thus resulting in the amplification of homochiral products (for clarity only ternary complexes are depicted). Peptide fragments are shown in helical conformation and represented as cylinders. Light and dark backgrounds denote regions of the sequence composed of L- and D-amino acids, respectively.

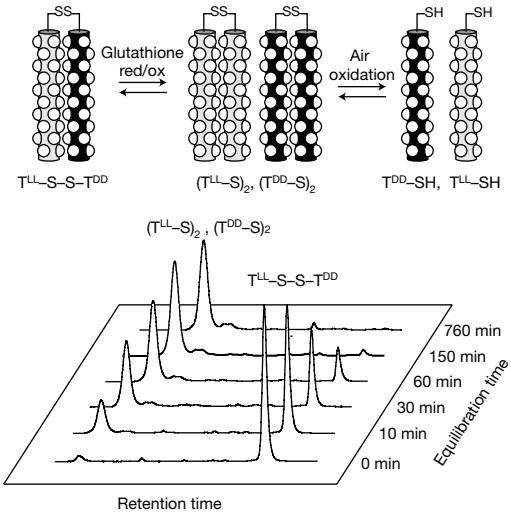

Figure 4 Schematic representation of chiroselective coiled-coil formation processes and the corresponding experimental HPLC time traces. Preformed heterochiral disulphide dimer $T^{DD}S–ST^{LL}$ (21.5 μM) in a glutathione redox buffer (500 μM reduced glutathione, 125 μM oxidized glutathione, 2 M NaCl, 100 mM MOPS buffer pH 7.5) undergoes complete disproportionation into homochiral assemblies $T^{LL}S–ST^{LL}$ and $T^{DD}S–ST^{DD}$, as indicated by the RP-HPLC time traces, which suggests that coiled-coil formation is intrinsically chiroselective.

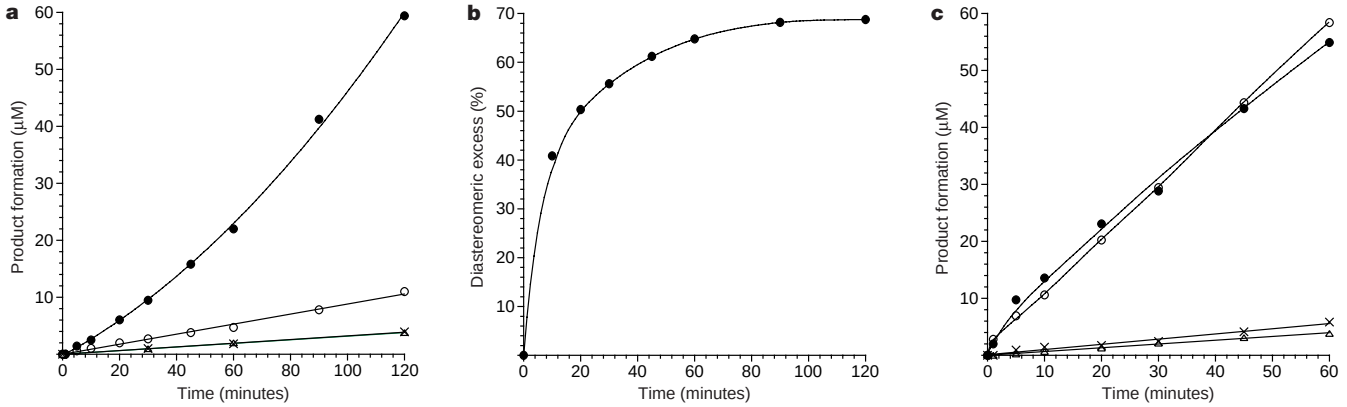

Figure 3 Rates of product formation with time. **a**, Template-directed chiroselective amplification. Production of homochiral products T^{LL} and T^{DD} (filled circles) and heterochiral products T^{LD} and T^{DL} (empty circles) is shown as a function of time for a reaction mixture containing 100-μM concentrations of each of fragments N^L, N^D, E^D and E^L. Production rates are shown for homochiral (empty triangle) and heterochiral products (cross) in a similar reaction mixture but in the presence of 3 M GndHCl. **b**, Increasing diastereomeric excess $100 \times [(T^{LL} + T^{DD}) - (T^{DL} + T^{LD})]/T^{total}$ as a function of time signifying amplification of homochiral products (data taken from Fig. 3a). **c**, Absence of enantiomeric cross-inhibition in chiroselective peptide replication and (auto)catalytic inactivity of heterochiral templates. Production of homochiral product T^{LL} in a reaction mixture containing 100 μM concentration of each fragment E^L and N^L is shown, in the presence of 25 μM initial concentration of T^{LL} (open circles) or in the presence of 25 μM initial concentrations of each of the products T^{LL}, T^{DD}, T^{DL} and T^{DL} (filled circles). Production rates of heterochiral product T^{DL} in a reaction mixture containing 100 μM concentration of fragments E^D and N^L are shown, in the presence (open triangle) or absence (cross) of 25 μM initial concentration of T^{LL}, T^{DD}, T^{DL} and T^{DL}. The lines are solely intended as a visual guide. All reactions, unless noted, were performed in 100 mM MOPS, 2 M NaCl, 1% v/v BnSH, pH 7.5 as described previously[17,18]. MOPS, 3-(N-morpholino)-propanesulphonic acid.

To investigate the thermodynamic basis of the chiroselective peptide self-replication process, the stereoselectivity in coiled-coil dimer formation[22] was studied by employing two enantiomeric homochiral templates, T^{DD}–SH and T^{LL}–SH. These peptides differ in sequence from T^{LL} and T^{DD} by only a Cys18Ser mutation and a Gly–Gly–Cys appendage at the amino terminus. The flexible appendage was employed to allow the formation of disulphide linked coiled coils[23] and the Cys18Ser mutation to ensure regioselectivity in disulphide bond-forming reactions (see below). The stereospecificity of coiled-coil formation was studied by allowing the racemic mixture of T^{DD}–SH and T^{LL}–SH to undergo slow air oxidation (25 μM each fragment in 100 mM MOPS, 2 M NaCl, pH 7.5) or by promoting disulphide exchange with preformed heterochiral disulphide-bonded dimer $T^{DD}S$–ST^{LL} in a glutathione redox buffer (Fig. 4a). HPLC analyses show that both the racemic mixture of T^{DD}–SH and T^{LL}–SH and the heterochiral dimer, $T^{DD}S$–ST^{LL}, are cleanly and quantitatively converted to the homochiral dimers, $T^{LL}S$–ST^{LL} and $T^{DD}S$–ST^{DD} (Fig. 4b), showing the same selectivity seen in the autocatalytic reactions. These results support the notion that the selectivity in autocatalytic fragment condensation is driven by the same homochiral molecular recognition events that favour the formation of the homochiral coiled-coils.

The limits of chiroselective amplification were tested by probing the effects of single amino acid stereochemical mutations within otherwise homochiral peptide fragments. Three nucleophilic peptide fragments $N^{L}_{dLeu\,26}$, $N^{L}_{dArg\,25}$ and $N^{L}_{dCys\,18}$ were prepared, each bearing a single D-amino acid substitution within the 15-residue homochiral nucleophilic fragment N^{L} (Fig. 1). The mutants $N^{L}_{dLeu\,26}$ and $N^{L}_{dArg\,25}$ were designed to test the effects of a stereochemical mutation within the informational complementary hydrophobic recognition interface and the non-informational solvent-exposed helical surface, respectively. Reaction mixtures containing equimolar amounts of E^{L} and either of the mutants $N^{L}_{dLeu\,26}$ or $N^{L}_{dArg\,25}$ produced only background rates of the corresponding fragment condensation products $T^{LL}_{dLeu\,26}$ and $T^{LL}_{dArg\,25}$, either in the presence or absence of 25 mole% of the template T^{LL}. Moreover, neither $T^{LL}_{dLeu\,26}$ nor $T^{LL}_{dArg\,23}$ were autocatalytically active. The third peptide fragment $N^{LL}_{dCys\,18}$ was designed to provide the most stringent test of chiroselectivity, because changing the chirality of the N-terminal residue was expected to have a minimal effect on the stability of the nascent helical fragment in solution or on its interactions with the template. Reaction mixtures containing equimolar amounts of E^{L} and $N^{L}_{dCys\,18}$ and 50 mole% of either T^{LL} or $T^{LL}_{dCys\,18}$ yielded a small rate enhancement in the formation of product $T^{LL}_{dCys\,18}$ (1.3 times over the background). However, in a direct competition experiment employing a 100 μM of N^{L} and $N^{L}_{dCyc\,18}$, 50 μM of E^{L}, and 50 μM each of T^{LL} and $T^{LL}_{dCyc\,18}$, the homochiral peptide T^{LL} quickly became the dominant species in the reaction mixture owing to its faster rate of production (Fig. 5a). The above studies establish that chiroselectivity in peptide self-replication is remarkably robust, not favouring reactants and products that differ stereochemically by one amino acid out of 15 or 32 residues.

An unexpected result of the above studies was that the three single stereochemical mutant products $T^{LL}_{dLeu\,26}$, $T^{LL}_{dArg\,25}$ and $T^{LL}_{dCys\,18}$ are efficient catalysts for the template-directed production of T^{LL} (Fig. 5b). A similar effect was observed previously[20] and shown to be the result of an autocratic self-organized network through which closely related mutant peptides ('errors' produced through background fragment condensation reactions) act as specific catalysts for the production of the native replicator (see ref. 20 for a discussion of the thermodynamic factors that may cause such an effect). In the present case, the heterochiral mutants $T^{LL}_{dLeu\,26}$, $T^{LL}_{dArg\,25}$ and $T^{LL}_{dCys\,18}$ accelerate the rate of production of the homochiral replicator T^{LL} by coupling the mutant template-mediate cross-catalytic cycles to the

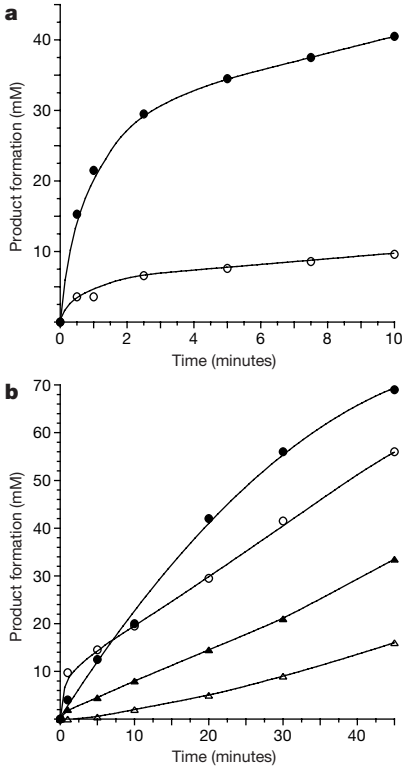

Figure 5 Rates of production formation in time. **a**, Probing the limits of chiroselective amplification through selective stereochemical mutations. Production of homochiral product T^{LL} (filled circles) and heterochiral product $T^{LL}_{dCys\,18}$ (open circle) are shown as a function of time in a reaction mixture containing equimolar (100 μM) concentration of competing fragments N^{L} and $N^{L}_{dCys\,18}$ and 50 μM concentrations of each of E^{L}, T^{LL}, and $T^{LL}_{dCys\,18}$ (production rates were quantitatively monitored by HPLC analyses of the depletion of N^{L} and $N^{L}_{dCyc\,18}$, owing to product peak overlaps). **b**, Heterochiral mutant products display a dynamic stereochemical editing function by cross-catalysing the production of the homochiral replicator sequence in a template-dependent fashion. Production of homochiral product T^{LL} in reaction mixtures containing 100 μM concentrations of N^{L} and E^{L} is efficiently catalysed in the presence of 50 μM initial concentrations of $T^{LL}_{dLeu\,26}$ (filled circle), $T^{LL}_{dCys\,18}$ (open circle) or $T^{LL}_{dArg\,25}$ (filled triangle). For comparison, the rate of production of T^{LL} in a similar reaction mixture but in the absence of added initial template is shown (open triangle). All reactions, unless noted, were performed in 100 mM MOPS, 2 M NaCl, 2 mM triscarboxyethyl phosphine, pH 7.5, as described previously[17,18].

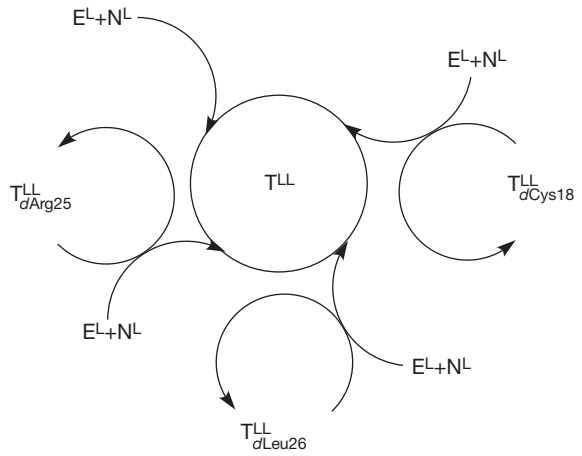

Figure 6 Schematic illustration of cross-catalytic networks established by heterochiral templates that help in the maintenance and amplification of homochiral products. The scheme depicts at the centre the autocatalytic cycle of homochiral replicator T^{LL} fed by the catalytic actions of three heterochiral single stereochemical mutant templates $T^{LL}_{dLeu\,26}$, $T^{LL}_{dCys\,18}$, and $T^{LL}_{dArg\,25}$. Overall, the system displays a dynamic stereochemical editing function as a result of the appearance of heterochiral sequences in the reaction mixture. For clarity, formation of mutant templates through uncatalysed background fragment condensation reactions is not shown.

autocatalytic production cycle of the homochiral template (Fig. 6). Cross-catalysis seems to result from the ability of these peptides to tolerate D-amino acid substitutions while maintaining a catalytically active conformation[24–26]. We refer to this process as 'dynamic stereochemical editing'.

Thus we have shown that even within the simple helical structure, a peptide replicator can contain a rich degree of information that enables it to display, at the molecular level, some of the basic characteristics of living systems, such as self-replication, homochirality, and resistance toward accumulation of errors (stereochemical mutations). The link between these traits allows the replicator to selectively amplify homochiral sequences. Therefore, chiroselectivity in peptide self-replication is a direct result of complementary noncovalent interactions that pass on both binding and stereochemical information simultaneously. That such a prototypical peptide system is able to amplify homochiral products through self-replication suggests that this and similar mechanisms may have affected the origin of homochirality on Earth. □

Received 19 October; accepted 8 December 2000.

1. Bonner, W. A. The origin and amplification of biomolecular chirality. *Origins Life Evol. Biosph.* **21,** 59–111 (1991).
2. Bada, J. L. Origins of homochirality. *Nature* **374,** 594–595 (1995).
3. Bonner, W. A., Blair, N. E. & Dirbas, F. M. Experiments on the abiotic amplification of optical activity. *Origins Life* **11,** 119–134 (1981).
4. Cronin, J. R. & Pizzarello, S. Enantiomeric excesses in meteoritic amino acids. *Science* **275,** 951–955 (1997).
5. Kondepudi, D. K. & Nelson, G. W. Weak neutral currents and the origin of biomolecular chirality. *Nature* **314,** 438–441 (1985).
6. Kondepudi, D. K., Kaufman, R. J. & Singh, N. Chiral symmetry breaking in sodium chlorate crystallization. *Science* **250,** 975–977 (1990).
7. Weissbuch, I. *et al.* Spontaneous generation and amplification of optical activity in .alpha.-amino acids by enantioselective occlusion into centrosymmetric crystals of glycine. *Nature* **310,** 161–164 (1984).
8. Frank, F. C. On spontaneous asymmetric synthesis. *Biochim. Biophys. Acta* **11,** 459–463 (1953).
9. Calvin, M. *Chemical Evolution* (Oxford Univ. Press, Oxford, 1969).
10. Girdard, C. & Kagan, H. B. Nonlinear effects in asymmetric synthesis and stereoselective reactions: ten years of investigation. *Angew. Chem. Int. Edn Engl.* **37,** 2923–2959 (1998).
11. Soai, K., Shibata, T., Morioka, H. & Choji, K. Asymmetric autocatalysis and amplification of enantiomeric excess of a chiral molecule. *Nature* **378,** 767–768 (1995).
12. Siegel, J. S. Homochiral imperative of molecular evolution. *Chirality* **10,** 24–27 (1998).
13. Bolli, M., Micura, R. & Eschenmoser, A. Pyranosyl-RNA: chiroselective self-assembly of base sequences by ligative oligomerization of tetranucleotide-2′,3′-cyclophosphates (with a commentary concerning the origin of biomolecular homochirality). *Chem. Biol.* **4,** 309–320 (1997).
14. Joyce, G. F. *et al.* Chiral selection in poly(C)-directed synthesis of oligo(G). *Nature* **310,** 602–604 (1984).
15. Schmidt, J. G., Nielsen, P. E. & Orgel, L. E. Enantiomeric cross-inhibition in the synthesis of oligonucleotides on a nonchiral template. *J. Am. Chem. Soc.* **119,** 1494–1495 (1997).
16. Kozlov, I. A., Politis, P. K., Pitsch, S., Herdewijn, P. & Orgel, L. E. A highly enantio-selective hexitol nucleic acid template for nonenzymic oligoguanylate synthesis. *J. Am. Chem. Soc.* **121,** 1108–1109 (1999).
17. Lee, D. H., Granja, J. R., Martinez, J. A., Severin, K. & Ghadiri, M. R. A self-replicating peptide. *Nature* **382,** 525–528 (1996).
18. Severin, K., Lee, D. H., Martinez, J. A. & Ghadiri, M. R. Peptide self-replication via template-directed ligation. *Chem. Eur. J.* **3,** 1017–1024 (1997).
19. Lee, D. H., Severin, K., Yokobayashi, Y. & Ghadiri, M. R. Emergence of symbiosis in peptide self-replication through a hypercyclic network. *Nature* **390,** 591–594 (1997).
20. Severin, K., Lee, D. H., Martinez, J. A., Vieth, M. & Ghadiri, M. R. Dynamic error correction in autocatalytic peptide networks. *Angew. Chem. Int. Edn Engl.* **37,** 126–128 (1998).
21. Li, T., Budt, K. H. & Kishi, Y. Influence of secondary structure (helical conformation) on stereoselectivity in peptide couplings. *J. Chem. Soc. Chem. Commun.* **24,** 1817–1819 (1987).
22. Case, M. A., Ghadiri, M. R., Mutz, M. W. & McLendon, G. L. Stereoselection in designed three-helix bundle metalloproteins. *Chirality* **10,** 35–40 (1998).
23. Harbury, P. B., Zhang, T., Kim, P. S. & Alber, T. A switch between two-, three-, and four-stranded coiled coils in GCN4 leucine zipper mutants. *Science* **262,** 1401–1407 (1993).
24. Krause, E., Bienert, M., Schmieder, P. & Wenshuh, H. The helix-destabilizing propensity scale of D-amino acids: the influence of side chain steric effects. *J. Am. Chem. Soc.* **122,** 4865–4870 (2000).
25. Rothemund, S. *et al.* Structure effects of double D-amino acid replacements: A nuclear magnetic resonance and circular dichroism study using amphipathic model helixes. *Biochemistry* **34,** 12954–12962 (1995).
26. Rothemund, S. *et al.* Peptide destabilization by two adjacent D-amino acids in single-stranded amphipathic alpha-helixes. *Pept. Res.* **9,** 78–87 (1996).
27. Dawson, P. E., Muir, T. W., Clark-Lewis, I. & Kent, S. B. H. Synthesis of proteins by native chemical ligation. *Science* **266,** 776–779 (1994).

Acknowledgements

We thank our colleagues A. Eschenmoser and L. Orgel for their helpful suggestions and critical review of this manuscript, and the NASA Astrobiology Institute for financial support.

Correspondence and requests for materials should be addressed to M.R.G. (e-mail: ghadiri@scripps.edu).

Evidence for non-selective preservation of organic matter in sinking marine particles

John I. Hedges*, Jeffrey A. Baldock†, Yves Gélinas*, Cindy Lee‡, Michael Peterson* & Stuart G. Wakeham§

* *School of Oceanography, Box 357940, University of Washington, Seattle, Washington 98195-7940, USA*
† *CSIRO Land and Water, PMB #2, Glen Osmond, South Australia 5064, Australia*
‡ *Marine Sciences Research Center, State University of New York, Stony Brook, New York 11794, USA*
§ *Skidaway Institute of Oceanography, 10 Ocean Science Circle, Savannah, Georgia 31411, USA*

The sinking of particulate organic matter from ocean surface waters transports carbon to the ocean interior[1,2], where almost all is then recycled. The unrecycled fraction of this organic matter can become buried in ocean sediments, thus sequestering carbon and so influencing atmospheric carbon dioxide concentrations[3]. The processes controlling the extensive biodegradation of sinking particles remain unclear, partly because of the difficulty in resolving the composition of the residual organic matter at depth with existing chromatographic techniques[4]. Here, using solid-state ^{13}C NMR spectroscopy[5], we characterize the chemical structure of organic carbon in both surface plankton and sinking particulate matter from the Pacific Ocean[4] and the Arabian Sea[6]. We found that minimal changes occur in bulk organic composition, despite extensive (>98%) biodegradation, and that amino-acid-like material predominates throughout the water column in both regions. The compositional similarity between phytoplankton biomass and the small remnant of organic matter reaching the ocean interior indicates that the formation of unusual biochemicals, either by chemical recombination[7] or microbial biosynthesis[8], is not the main process controlling the preservation of particulate organic carbon within the water column at these two sites. We suggest instead that organic matter might be protected from degradation by the inorganic matrix of sinking particles.

The ocean interior acts as a global heterotrophic digester, where almost all organic matter injected from surface (0–100 m) waters is respired to inorganic nutrients[2]. Such 'remineralization' is important because sinking organic particles selectively transport bioactive elements through density-stratified water columns typical of temperate oceans[1]. Although the size and density of sinking particles affect nutrient release at depth, reaction rates of the component biochemicals are also important considerations[9,10]. Unfortunately, the percentage of the total organic matter in this particle rain that can be molecularly characterized by conventional chromatographic analysis decreases rapidly down ocean water columns to become a minor component (<25%) at depth[4]. The attenuation of definitive molecular information with increasing ocean depth[11] greatly diminishes our understanding of the forms and reaction potentials of organic materials flowing through one of the most ecologically important, and climatically critical, transport pathways in the ocean[12].

Several hypotheses have been offered for the universally observed decrease in molecularly resolvable organic substances attending advanced biodegradation. The classical explanation is that labile intermediates released during microbial degradation of biomacromolecules (for example, polysaccharides, lignins and proteins) spontaneously recombine to form chemically complex "geopolymers"[7]. Products of such abiotic 'humification' reactions